Letter to the Editor

# Synchronous carotid body and anterior mediastinal paraganglioma revealed by $^{18}$F-fluorodeoxyglucose and $^{68}$Ga-DOTA(0)-Tyr(3)-octreotate positron emission tomography-computed tomography

**Hangyu Xie[#], Hua Lin[#], Lin Li[*], Wenjie Zhang[*]**

Department of Nuclear Medicine, West China Hospital of Sichuan University, Chengdu, China

[#]These authors contributed equally to this work and should be considered as co-first authors.

[*]These authors contributed equally to this work and should be considered as co-corresponding authors.

*Correspondence to:* Lin Li, MD; Wenjie Zhang, MD. Department of Nuclear Medicine, West China Hospital of Sichuan University, No. 37, Guoxue Alley, Chengdu 610041, China. Email: lilinhuaxi@sina.com; zhang_wenjie@stu.scu.edu.cn.

Submitted Sep 23, 2022. Accepted for publication Mar 15, 2023. Published online Apr 04, 2023.
doi: 10.21037/qims-22-1018
**View this article at:** https://dx.doi.org/10.21037/qims-22-1018

## Introduction

Paragangliomas (PGLs) are rare nonepithelial neuroendocrine neoplasms (NENs) (1,2). Synchronous PGLs in the neck and anterior mediastinum are highly rare. The present study describes how a synchronous carotid body and anterior mediastinal PGL was revealed with $^{18}$F-fluorodeoxyglucose ($^{18}$F-FDG) and $^{68}$Ga-DOTA(0)-Tyr(3)-octreotate ($^{68}$Ga-DOTATATE) positron emission tomography-computed tomography (PET-CT), which included using 2 types of quantitative imaging tracers. Different degrees of tracer accumulation were observed in 2 synchronous PGLs. Surgical resection of both lesions was performed. Histopathologic examination and immunohistochemistry of the neck and thoracic lesions confirmed the diagnosis of 2 primary synchronous PGLs.

## Case presentation

A 41-year-old man had a mass on the right side of the neck for 5 years. He reported a month of gradual expansion of the mass. There was a palpable, movable, tender mass with a diameter of approximately 4 cm. Deep pressure caused the patient to cough. The patient's 24-hour urinary dopamine level was 438.12 μg/24 hours (65–400 μg/24 hours), his homovanillic acid level was 13.64 μg/24 hours (0–8 μg/24 hours), and his vanillic acid level was 10.38 μg/24 hours (0–8 μg/24 hours). The patient's 24-hour urinary methoxynoradrenaline level was 30.14 μg/24 hours (103–560 μg/24 hours). His biochemical investigations, including blood catecholamine and metabolites, were within the normal range. Three-dimensional reconstruction of the neck vessels (*Figure 1A*) showed that this mass enclosed the right distal common carotid artery (CCA), the carotid bifurcation, the proximal internal carotid artery (ICA), and the external carotid artery (ECA). Contrast-enhanced computed tomography (CT; *Figure 1B*) showed a highly vascularized lesion measuring 4.7×4.1 cm in size on the right side of the upper neck, which was mainly located in the CCA region. The possibility of PGL was considered.

Subsequently, $^{18}$F-FDG and $^{68}$Ga-DOTATATE PET-CT scans were conducted to evaluate the presence of multifocal lesions or distant metastases. The whole-body maximum intensity projection (MIP) image revealed that the neck (*Figure 2A,2B*, short black arrow) and thoracic region (*Figure 2A,2B*, long black arrow) had a focal and increased FDG and DOTATATE uptake lesion, respectively. Axial CT of the neck showed a soft tissue lesion in the right upper neck region (*Figure 2C,2D*, short blue arrow) with moderate FDG accumulation [maximum standardized uptake value (SUVmax) of 3.92] and significantly intense DOTATATE accumulation (SUVmax of 51.0) on PET-CT fusion

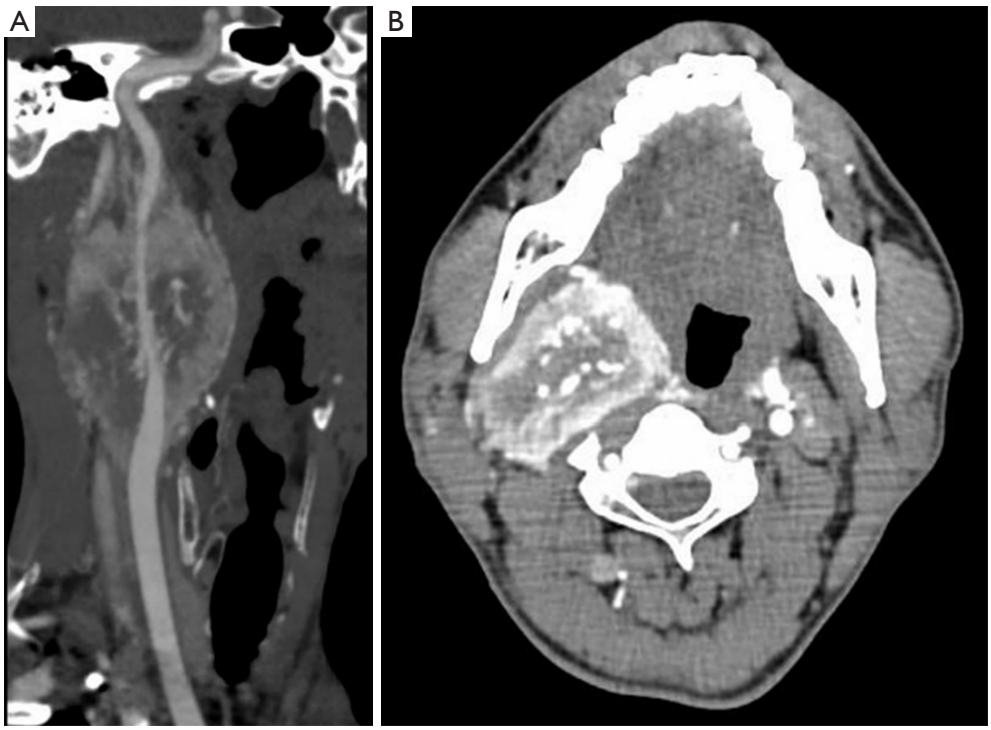


**Figure 1** A 3D reconstruction of vessels and the contrast-enhanced CT finding. (A) A 3D reconstruction of the cervical vessels showed a mass enclosing the right distal CCA, the carotid bifurcation, ICA, and ECA. (B) Contrast-enhanced CT showed a highly vascularized lesion on the right side of the upper neck. 3D, 3-dimensional; CT, computed tomography; CCA, common carotid artery; ICA, the proximal internal carotid artery; ECA, the external carotid artery.

images (*Figure 2E,2F*, long blue arrow) and PET images (*Figure 2G,2H*, orange arrow), respectively. Interestingly, axial CT of the anterior mediastinum showed an irregular soft tissue mass close to the ascending aorta (*Figure 2I,2J*, short white arrow) with intense FDG uptake (SUVmax 7.56) and relatively intense DOTATATE uptake (SUVmax 20.79) on PET-CT fusion images (*Figure 2K,2L*, long white arrow) and PET images (*Figure 2M,2N*, red arrow), respectively. Based on the above findings, it was suggested that the right neck mass was a PGL and that the anterior mediastinal mass was possibly another primary tumor. Right carotid body aneurysm resection and autologous saphenous vein bypass of the right common carotid-ICA were performed on August 20, 2021. Postoperatively, the patient presented with a slight tongue deviation to the right and experienced hoarseness, choking, or coughing while drinking water. Considering the patient's inability to tolerate joint cervical and thoracic surgery, subxiphoid video-assisted thoracic surgery thymectomy and anterior mediastinal mass resection were performed 4 months later on December 21, 2021. Serum and urine catecholamine metabolite levels were not rechecked postoperatively. No new complications occurred. Histopathologic examination of the neck and thoracic lesions confirmed the diagnosis of 2 primary synchronous PGLs (*Figure 3*; *Figure 4*), and immunohistochemical analysis of thoracic lesions showed that chromogranin A (CgA), S-100, and synaptophysin (Syn) were all positive (*Figure 4*). All procedures performed in this study were conducted in accordance with the ethical standards of the institutional and/or national research committee(s) and the Declaration of Helsinki (as revised in 2013). Written informed consent was provided by the patient to publish this case report and accompanying images. A copy of the written consent is available for review from the editorial office of this journal.

## Discussion

PGLs are rare neuroendocrine tumors arising from the extra-adrenal sympathetic or parasympathetic autonomic paraganglia (3). PGLs are usually located in the thoracolumbar sympathetic ganglia and the craniosacral parasympathetic nervous system (4). Therefore, PGLs can

 

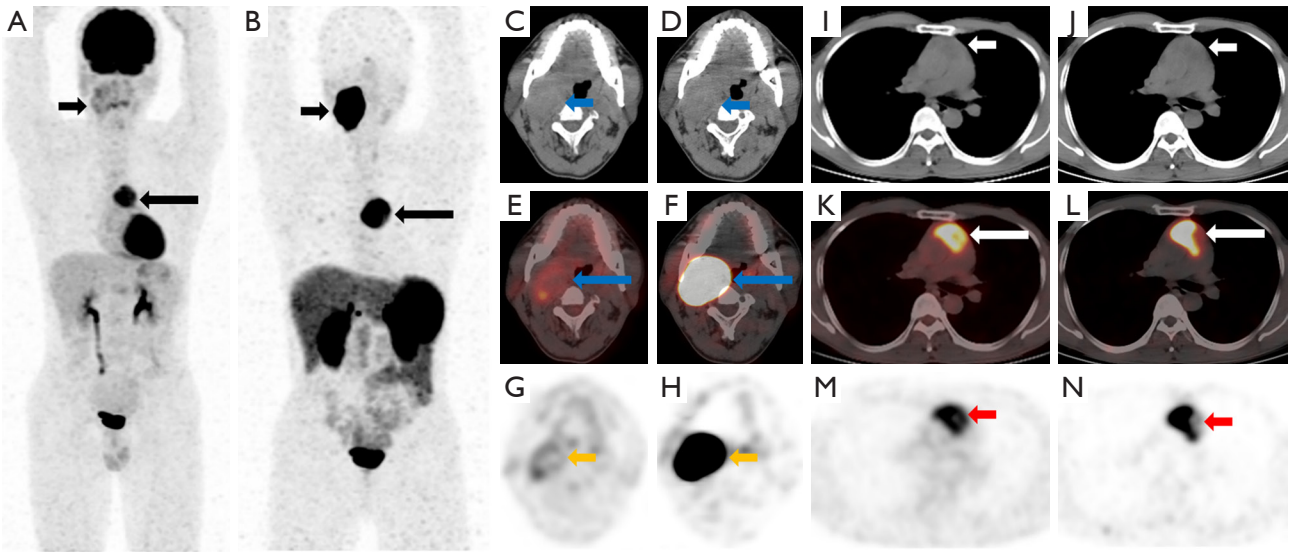


**Figure 2** $^{18}$F-FDG and $^{68}$Ga-DOTATATE PET-CT imaging of the right upper neck and the anterior mediastinum lesions. (A,B) MIP. The short black arrow indicates the neck region, and the long black arrow indicates the thoracic region). (C,D: short blue arrow) Axial CT of the neck and chest. (E,F: long blue arrow) FDG PET-CT fusion images. (G,H: orange arrow) PET imaging. (I,J: short white arrow) Axial CT of the chest. (K,L: long white arrow) DOTATATE PET-CT fusion imaging. (M,N: red arrow) PET imaging revealed a soft tissue mass in the right neck and anterior mediastinum with increased $^{18}$F-FDG and $^{68}$Ga-DOTATATE uptake. $^{18}$F-FDG, $^{18}$F-fluorodeoxyglucose; $^{68}$Ga-DOTATATE, $^{68}$Ga-DOTA(0)-Tyr(3)-octreotate; PET-CT, positron emission tomography-computed tomography; MIP, maximum intensity projection.

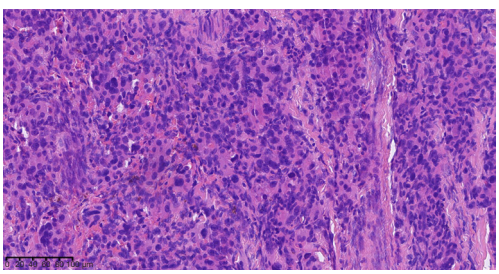

**Figure 3** The pathology of the tumor showed carotid body paraganglioma. HE staining showed that the tumor was composed of nests of cells arranged in a classic Zellballen pattern with abundant blood sinuses between cell nests (magnification ×200). No immunohistochemical staining was performed for this lesion. HE, hematoxylin and eosin.

appear in the abdomen, pelvis, head, neck, and thorax (5). Most PGLs are isolated, benign, and nonfunctional. PET-CT findings of solitary PGLs involving the carotid body, jugular, tympanic tumor, urinary bladder, mediastinum, pulmonary, spinal canal, atrial, and epicardial have been reported (6). Synchronous PGLs usually occur in the head and neck region, accounting for approximately 10–22% of sporadic or nonfamilial cases (7-11). Coexistence in the neck and anterior mediastinal PGLs is rare. To date, 8 cases (not including the present case) of synchronous neck and chest PGLs have been reported (12-19). The demographic, clinical, and tumor characteristics of these cases are summarized in *Table 1*. Among all these cases, most patients were middle-aged males with or without hypertension. The patients' ages ranged from 30 to 58 years. The maximum diameter of the tumor was 8 cm. The clinical presentation of PGLs depends on the symptoms caused by excessive catecholamine secretion. Typical symptoms are headaches, palpitations, and profuse sweating. Synchronous cervical-thoracic PGLs reported in the literature are usually closely associated with the middle mediastinum. We here report the $^{18}$F-FDG and $^{68}$Ga-DOTATATE PET-CT findings for a case of synchronous carotid body and anterior mediastinum PGL.

Anatomical imaging, such as ultrasound, CT, and magnetic resonance imaging (MRI), has been used to evaluate PGLs. Contrast-enhanced CT or MRI provides lesion-enhancing details and can reveal the relationship between lesions and the surrounding blood vessels. Functional imaging, such as $^{18}$F-FDG PET, $^{68}$Ga-

 

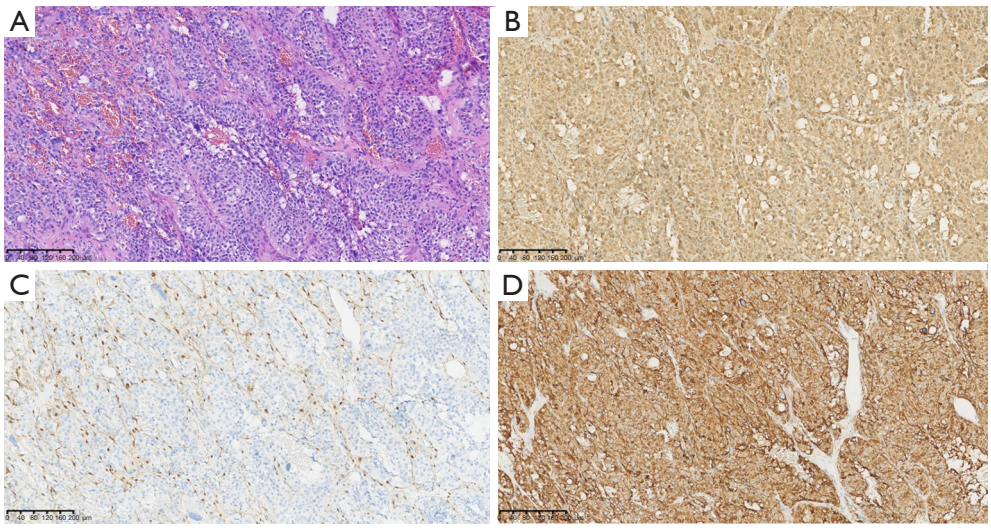


**Figure 4** The pathology of the tumor showing anterior mediastinal paraganglioma. (A) HE staining showed that the tumor was composed of nests of cells arranged in a classic Zellballen pattern with abundant blood sinuses between cell nests (magnification ×200). (B-D) Immunohistochemical staining showed CgA, S-100, and Syn positivity (+) in tumor cells (magnification ×100). HE, hematoxylin and eosin; CgA, chromogranin A; Syn, synaptophysin.

DOTA-somatostatin analog (SSA) PET, 3,4-dihydroxy-6-[18F]-fluoro-L-phenylalanine ($^{18}$F-DOPA) PET, $^{123}$I-metaiodobenzylguanidine ($^{123}$I-MIBG) single-photon emission computed tomography (SPECT), and $^{111}$In-pentetreotide/octreotide SPECT imaging, plays a crucial role in the detection, staging, therapeutic response assessment, and determination of suitability for peptide-based radioreceptor therapy in patients with PGLs (20-23). Generally, PET imaging is more sensitive than is SPECT imaging. $^{68}$Ga-DOTATATE has a high affinity for somatostatin receptor 2 (SSTR2), which is overexpressed in most PGLs. $^{68}$Ga-DOTA-SSA PET imaging has been recommended as a first-line imaging method for PGLs, especially metastatic PGLs. $^{18}$FDG PET-CT is recommended as a second-line imaging method (24-27). $^{68}$Ga-DOTA-SSA demonstrates superior lesion detectability for PGLs over other functional and anatomic imaging modalities. Tan *et al.* (28) showed that $^{68}$Ga-DOTATATE PET-CT (92.6%) was the most sensitive imaging modality in mapping PGLs and related lesions compared with $^{18}$F-FDG PET-CT (57.8%) and $^{131}$I-MIBG (26.0%) scintigraphy on a per-lesion basis, which was similar to the findings of other studies (29-31). Several studies that evaluated PGLs revealed significantly higher lesion detectability of $^{68}$Ga-DOTATATE PET-CT (98.6–100%) over CT and MRI (60.5–84.8%) (32-34).

The development of molecular imaging and tracers provides insights into intratumoral or intertumoral heterogeneity and shows the advantage of uncovering spatiotemporal heterogeneity (35). Understanding this remarkable biological heterogeneity helps us to gain insight into the clinical manifestations and disease course, which can guide clinical treatment decisions and assist in evaluating prognoses (36). Due to the differences in radiopharmaceutical avidity and imaging modalities in our case, the cervical lesions (Ki-67 5%) showed mild FDG uptake but significantly intense DOTATATE uptake. In contrast, the anterior mediastinal lesions (Ki-67 20%) showed increased FDG uptake and more intense DOTATATE uptake. The size of the 2 lesions on DOTATATE PET images was even larger than that of those on FDG PET images. The distinct imaging characteristics suggested tumor heterogeneity, which might have been related to the degree of cell proliferation index (Ki-67), tumor metabolic activity, and somatostatin receptor density.

PGL is a highly vascularized tumor in which the carotid body tumor is located at the carotid bifurcation and has classic radiographic features; that is, a homogeneously enhancing soft tissue mass can be seen at the carotid bifurcation on contrast-enhanced CT with splaying of the ICA and ECA, and the carotid bifurcation appears in

 

**Table 1** Demographic, clinical, and tumor characteristics of 8 reported cases of synchronous neck and chest PGLs

| Publication [year] | Age (years) | Gender | Signs and symptoms | Previous history | Tumor location (size) | Imaging modality |
|---|---|---|---|---|---|---|
| Reinert [2000] (12) | 47 | Male | Progressive swelling of the bilateral neck | NA | Jugular regions and anterior mediastinum | Contrast-enhanced CT and angiography |
| Taïeb [2014] (13) | NA | NA | NA | NA | Right carotid body and mediastinum | Somatostatin receptor SPECT and $^{18}$F-FDG PET/CT |
| Witkowska [2014] (14) | 37 | Male | NA | Multiorgan sarcoidosis and hypertension | Retroperitoneal (4 cm), mediastinum, neck (bilaterally), and right jugular foramen | Contrast-enhanced CT, MRI, $^{68}$Ga DOTATATE PET-CT and $^{123}$I-MIBG SPECT |
| Stratakis [2014] (15) | 37 | Male | Recurrent generalized headaches and visual difficulties | Hypertension | Bilateral carotid area, epicardial and paravertebral mass at the T6/T7 level | $^{123}$I-MIBG, $^{111}$In-pentetreotide SPECT and $^{18}$F-FDG PET/CT |
| Massad [2017] (16) | 30 | Male | Neck mass and palpitations | NA | Right carotid body bifurcation (3.0×8.0 cm) and left atrial | Cardiac MRI, contrast-enhanced CT and $^{123}$I-MIBG SPECT |
| Inoue [2017] (17) | 58 | Female | NA | Resection of carotid body tumor and hypertension | Left atrium (5.6×5.1 cm) | Echocardiography, contrast-enhanced CT and MRI |
| Shu [2020] (18) | 46 | Male | Recurrent chest pain | Resection of bilateral carotid artery PGL | Right atrioventricular groove (3.0×2.5×2.0 cm) | Echocardiography, coronary angiography, and $^{18}$F-FDG PET-CT |
| Dhirawani [2021] (19) | 42 | Male | Breathlessness, chest pain, and excessive perspiration | Hypertension | Left para-aortic region (4.1×2.8×2.9 cm) and left common carotid artery (1.7×1.5×1.1 cm) | Contrast-enhanced CT, echocardiography, and $^{18}$F-FDG PET-CT |

PGLs, paragangliomas; NA, not available; CT, computed tomography; SPECT, single-photon emission computed tomography; $^{18}$F-FDG, $^{18}$F-fluorodeoxyglucose; $^{68}$Ga-DOTATATE, $^{68}$Ga-DOTA(0)-Tyr(3)-octreotate; PET-CT, positron emission tomography-computed tomography; $^{123}$I-MIBG, $^{123}$I-metaiodobenzylguanidine; MRI, magnetic resonance imaging.

a typical "goblet deformity"; meanwhile, MRI shows a hyperintense lesion in T2-weighted imaging and the typical "salt and pepper effect" appearance comprising low signal flow voids and high signal foci of hemorrhage (37). The differential diagnosis of an anterior mediastinal mass most often includes thymoma, teratoma, thyroid disease, and lymphoma (38). Anterior mediastinal PGLs show intense DOTATATE uptake, while other anterior mediastinal masses often have a background or mild to moderate DOTATATE uptake (6). PGLs should be considered when certain paraganglia sites have different degrees of FDG or DOTATATE uptake.

## Conclusions

The present case report the use of $^{18}$F-FDG and $^{68}$Ga DOTATATE PET-CT for detecting synchronous PGLs. Moreover, our report shows that different degrees of FDG and DOTATATE uptake can occur at different sites of PGLs. These findings further our understanding the of metabolic differences in PGLs and provide quantitative information related to tumor biological aggressiveness and somatostatin expression levels.

## Acknowledgments

*Funding:* The research was supported by the 1.3.5 Project for Disciplines of Excellence; the West China Hospital, Sichuan University (No. ZYGD18016); and the Sichuan Science and Technology Program (No. 2022YFH0047).

## Footnote

*Conflicts of Interest:* All authors have completed the ICMJE uniform disclosure form (available at https://qims.amegroups.com/article/view/10.21037/qims-22-1018/coif). The authors report that this research was supported by the 1.3.5 Project for Disciplines of Excellence, West China Hospital, Sichuan University (No. ZYGD18016), and the Sichuan Science and Technology Program (No. 2022YFH0047). The authors have no other conflicts of interest to declare.

*Ethical Statement:* The authors are accountable for all aspects of the work in ensuring that questions related to the accuracy or integrity of any part of the work are appropriately investigated and resolved. All procedures performed in this study were conducted in accordance with the ethical standards of the institutional and/or national research committee(s) and with the Helsinki Declaration (as revised in 2013). Written informed consent was obtained from the patient to publish this case report and accompanying images. A copy of the written consent is available for review by the editorial office of this journal.



## References

1. Mete O, Asa SL, Gill AJ, Kimura N, de Krijger RR, Tischler A. Overview of the 2022 WHO Classification of Paragangliomas and Pheochromocytomas. Endocr Pathol 2022;33:90-114.
2. Mercado-Asis LB, Wolf KI, Jochmanova I, Taïeb D. Pheochromocytoma: a genetic and diagnostic update. Endocr Pract 2018;24:78-90.
3. Garcia-Carbonero R, Matute Teresa F, Mercader-Cidoncha E, Mitjavila-Casanovas M, Robledo M, Tena I, Alvarez-Escola C, Arístegui M, Bella-Cueto MR, Ferrer-Albiach C, Hanzu FA. Multidisciplinary practice guidelines for the diagnosis, genetic counseling and treatment of pheochromocytomas and paragangliomas. Clin Transl Oncol 2021;23:1995-2019.
4. Kim, Lee IJ, Park MC, Kim JH, Lim H. Cutaneous paraganglioma of the vertex in a child. J Craniofac Surg 2012;23:e338-40.
5. Lenders JW, Eisenhofer G, Mannelli M, Pacak K. Phaeochromocytoma. Lancet 2005;366:665-75.
6. Dudgeon MG, Sonavane SK, Parent EE, Khoor A, Thomas M. Co-existent Epicardial Paraganglioma and Anterior Mediastinal Thymoma. J Radiol Case Rep 2020;14:16-30.
7. Netterville JL, Jackson CG, Miller FR, Wanamaker JR, Glasscock ME. Vagal paraganglioma: a review of 46 patients treated during a 20-year period. Arch Otolaryngol Head Neck Surg 1998;124:1133-40.
8. Urquhart AC, Johnson JT, Myers EN, Schechter GL. Glomus vagale: paraganglioma of the vagus nerve.

 

Laryngoscope 1994;104:440-5.
9. Szymańska A, Szymański M, Czekajska-Chehab E, Goł bek W, Szczerbo-Trojanowska M. Diagnosis and management of multiple paragangliomas of the head and neck. Eur Arch Otorhinolaryngol 2015;272:1991-9.
10. Thabet MH, Kotob H. Cervical paragangliomas: diagnosis, management and complications. J Laryngol Otol 2001;115:467-74.
11. Papaspyrou K, Mewes T, Rossmann H, Fottner C, Schneider-Raetzke B, Bartsch O, Schreckenberger M, Lackner KJ, Amedee RG, Mann WJ. Head and neck paragangliomas: Report of 175 patients (1989-2010). Head Neck 2012;34:632-7.
12. Hoffmann J, Kröber SM, Hahn U, Ernemann U, Reinert S. Polytopic manifestations of paragangliomas. Diagnosis, differential diagnosis and indications for therapy. Mund Kiefer Gesichtschir 2000;4:53-6.
13. Blanchet EM, Gabriel S, Martucci V, Fakhry N, Chen CC, Deveze A, Millo C, Barlier A, Pertuit M, Loundou A, Pacak K, Taïeb D. 18F-FDG PET/CT as a predictor of hereditary head and neck paragangliomas. Eur J Clin Invest 2014;44:325-32.
14. Kunikowska J, Grabowska L, Toutounchi S, Cieszanowski A, Witkowska M. Retroperitoneal pheochromocytoma with thorax and bilateral neck chemodectoma in patients with multiorgan sarcoidosis. Clin Nucl Med 2014;39:e258-62.
15. Skoura E, Datseris IE, Xekouki P, Tolis G, Stratakis CA. SPECT and 18F-FDG PET/CT imaging of multiple paragangliomas and a growth hormone-producing pituitary adenoma as phenotypes from a novel succinate dehydrogenase subunit D mutation. Clin Nucl Med 2014;39:81-3.
16. Abdelhady K, Durgam S, Orza D, Massad MG. Left Atrial and Carotid Body Paraganglioma. Ann Thorac Surg 2017;103:e323-5.
17. Otani N, Sugano K, Inami S, Amano H, Arikawa T, Saito S, Imai K, Ushiama M, Yoshida T, Kimura N, Toyoda S, Inoue T. Cardiac paraganglioma with a novel germline mutation of succinate dehydrogenase gene D. Jpn J Clin Oncol 2017;47:1193-7.
18. Wang Q, Huang ZY, Ge JB, Shu XH. Nonhypertensive male with multiple paragangliomas of the heart and neck: A case report. World J Clin Cases 2020;8:5707-14.
19. Kalekar T, Rangankar V, Ayapaneni DR, Chanabasanavar V, Dhirawani S. Multiple Paragangliomas in the Carotid Body, Adrenal and Extra-Adrenal Retroperitoneal Locations. Cureus 2021;13:e18258.
20. Carrasquillo JA, Chen CC, Jha A, Ling A, Lin FI, Pryma DA, Pacak K. Imaging of Pheochromocytoma and Paraganglioma. J Nucl Med 2021;62:1033-42.
21. Ryder SJ, Love AJ, Duncan EL, Pattison DA. PET detectives: Molecular imaging for phaeochromocytomas and paragangliomas in the genomics era. Clin Endocrinol (Oxf) 2021;95:13-28.
22. Fortunati E, Argalia G, Zanoni L, Fanti S, Ambrosini V. New PET Radiotracers for the Imaging of Neuroendocrine Neoplasms. Curr Treat Options Oncol 2022;23:703-20.
23. Taïeb D, Hicks RJ, Hindié E, Guillet BA, Avram A, Ghedini P, Timmers HJ, Scott AT, Elojeimy S, Rubello D, Virgolini IJ, Fanti S, Balogova S, Pandit-Taskar N, Pacak K. European Association of Nuclear Medicine Practice Guideline/Society of Nuclear Medicine and Molecular Imaging Procedure Standard 2019 for radionuclide imaging of phaeochromocytoma and paraganglioma. Eur J Nucl Med Mol Imaging 2019;46:2112-37.
24. Lin EP, Chin BB, Fishbein L, Moritani T, Montoya SP, Ellika S, Newlands S. Head and Neck Paragangliomas: An Update on the Molecular Classification, State-of-the-Art Imaging, and Management Recommendations. Radiol Imaging Cancer 2022;4:e210088.
25. Bozkurt MF, Virgolini I, Balogova S, Beheshti M, Rubello D, Decristoforo C, Ambrosini V, Kjaer A, Delgado-Bolton R, Kunikowska J, Oyen WJG, Chiti A, Giammarile F, Sundin A, Fanti S. Erratum to: Guideline for PET/CT imaging of neuroendocrine neoplasms with (68) Ga-DOTA-conjugated somatostatin receptor targeting peptides and (18)F-DOPA. Eur J Nucl Med Mol Imaging 2017;44:2150-1.
26. Zandee WT, de Herder WW. The Evolution of Neuroendocrine Tumor Treatment Reflected by ENETS Guidelines. Neuroendocrinology 2018;106:357-65.
27. Sundin A, Arnold R, Baudin E, Cwikla JB, Eriksson B, Fanti S, Fazio N, Giammarile F, Hicks RJ, Kjaer A, Krenning E, Kwekkeboom D, Lombard-Bohas C, O'Connor JM, O'Toole D, Rockall A, Wiedenmann B, Valle JW, Vullierme MP; Antibes Consensus Conference participants. ENETS Consensus Guidelines for the Standards of Care in Neuroendocrine Tumors: Radiological, Nuclear Medicine & Hybrid Imaging. Neuroendocrinology 2017;105:212-44.
28. Tan TH, Hussein Z, Saad FF, Shuaib IL. Diagnostic Performance of (68)Ga-DOTATATE PET/CT, (18) F-FDG PET/CT and (131)I-MIBG Scintigraphy in Mapping Metastatic Pheochromocytoma and

 

Paraganglioma. Nucl Med Mol Imaging 2015;49:143-51.
29. Maurice JB, Troke R, Win Z, Ramachandran R, Al-Nahhas A, Naji M, Dhillo W, Meeran K, Goldstone AP, Martin NM, Todd JF, Palazzo F, Tan T. A comparison of the performance of $^{68}$Ga-DOTATATE PET/CT and $^{123}$I-MIBG SPECT in the diagnosis and follow-up of phaeochromocytoma and paraganglioma. Eur J Nucl Med Mol Imaging 2012;39:1266-70.
30. Dodamani MH, Jaiswal SK, Sarathi V, Marfatia H, D'Cruz A, Malhotra G, Hira P, Patil VA, Lila AR, Shah NS, Bandgar TR. Comparison of the Sensitivity of (68) Ga-DOTATATE PET/CT with Other Imaging Modalities in Detecting Head and Neck Paraganglioma: Experience from Western India. World J Nucl Med 2022;21:184-91.
31. Chang CA, Pattison DA, Tothill RW, Kong G, Akhurst TJ, Hicks RJ, Hofman MS. (68)Ga-DOTATATE and (18)F-FDG PET/CT in Paraganglioma and Pheochromocytoma: utility, patterns and heterogeneity. Cancer Imaging 2016;16:22.
32. Janssen I, Blanchet EM, Adams K, Chen CC, Millo CM, Herscovitch P, Taieb D, Kebebew E, Lehnert H, Fojo AT, Pacak K. Superiority of [68Ga]-DOTATATE PET/CT to Other Functional Imaging Modalities in the Localization of SDHB-Associated Metastatic Pheochromocytoma and Paraganglioma. Clin Cancer Res 2015;21:3888-95.
33. Janssen I, Chen CC, Taieb D, Patronas NJ, Millo CM, Adams KT, Nambuba J, Herscovitch P, Sadowski SM, Fojo AT, Buchmann I, Kebebew E, Pacak K. 68Ga-DOTATATE PET/CT in the Localization of Head and Neck Paragangliomas Compared with Other Functional Imaging Modalities and CT/MRI. J Nucl Med 2016;57:186-91.
34. Patel M, Jha A, Ling A, Chen CC, Millo C, Kuo MJM, Nazari MA, Talvacchio S, Charles K, Miettinen M, Del Rivero J, Chen AP, Nilubol N, Lin FI, Civelek AC, Taïeb D, Carrasquillo JA, Pacak K. Performances of Functional and Anatomic Imaging Modalities in Succinate Dehydrogenase A-Related Metastatic Pheochromocytoma and Paraganglioma. Cancers (Basel) 2022;14:3886.
35. Crona J, Backman S, Maharjan R, Mayrhofer M, Stålberg P, Isaksson A, Hellman P, Björklund P. Spatiotemporal Heterogeneity Characterizes the Genetic Landscape of Pheochromocytoma and Defines Early Events in Tumorigenesis. Clin Cancer Res 2015;21:4451-60.
36. Iravani A, Parihar AS, Akhurst T, Hicks RJ. Molecular imaging phenotyping for selecting and monitoring radioligand therapy of neuroendocrine neoplasms. Cancer Imaging 2022;22:25.
37. Berger G, Łukasiewicz A, Grinevych V, Tarasów E. Carotid Body Tumor – radiological imaging and genetic assessment. Pol Przegl Chir 2020;92:39-44.
38. Duwe BV, Sterman DH, Musani AI. Tumors of the mediastinum. Chest 2005;128:2893-909.

**Cite this article as:** Xie H, Lin H, Li L, Zhang W. Synchronous carotid body and anterior mediastinal paraganglioma revealed by $^{18}$F-fluorodeoxyglucose and $^{68}$Ga-DOTA(0)-Tyr(3)-octreotate positron emission tomography-computed tomography. Quant Imaging Med Surg 2023;13(6):4007-4014. doi: 10.21037/qims-22-1018

 